AFRL-RZ-WP-TP-2008-2067

AERODYNAMIC PERFORMOANCE OF AN INJECTOR STRUT FOR A ROUND SCRAMJET COMBUSTOR (POSTPRINT)

Chung-Jen Tam, Kuang-Yu Hsu, Mark R. Gruber, and Charbel N. Raffoul

Propulsion Sciences Branch
Aerospace Propulsion Division

JULY 2007
Interim Report

AIR FORCE RESEARCH LABORATORY
PROPULSION DIRECTORATE
WRIGHT-PATTERSON AIR FORCE BASE, OH 45433-7251
AIR FORCE MATERIEL COMMAND
UNITED STATES AIR FORCE

REPORT DOCUMENTATION PAGE

Form Approved
OMB No. 0704-0188

1. REPORT DATE *(DD-MM-YY)*	2. REPORT TYPE	3. DATES COVERED *(From - To)*
July 2007	Conference Paper Postprint	01 August 2006 – 31 July 2007

4. TITLE AND SUBTITLE

AERODYNAMIC PERFORMOANCE OF AN INJECTOR STRUT FOR A ROUND SCRAMJET COMBUSTOR (POSTPRINT)

5a. CONTRACT NUMBER
IN HOUSE

5b. GRANT NUMBER

5c. PROGRAM ELEMENT NUMBER
62203F

6. AUTHOR(S)

Chung-Jen Tam, Kuang-Yu Hsu, and Mark R. Gruber (Propulsion Sciences Branch, Aerospace Propulsion Division (AFRL/RZAS))
Charbel N. Raffoul (Propulsion Technology Branch, Aerospace Propulsion Division (AFRL/RZAT))

5d. PROJECT NUMBER
3012

5e. TASK NUMBER
AI

5f. WORK UNIT NUMBER
3012AI00

7. PERFORMING ORGANIZATION NAME(S) AND ADDRESS(ES)

Propulsion Sciences Branch
Aerospace Propulsion Division
Air Force Research Laboratory, Propulsion Directorate
Wright-Patterson Air Force Base, OH 45433-7251
Air Force Materiel Command, United States Air Force

Propulsion Technology Branch,
Aerospace Propulsion Division
(AFRL/RZAT)

8. PERFORMING ORGANIZATION REPORT NUMBER
AFRL-RZ-WP-TP-2008-2067

9. SPONSORING/MONITORING AGENCY NAME(S) AND ADDRESS(ES)

Air Force Research Laboratory
Propulsion Directorate
Wright-Patterson Air Force Base, OH 45433-7251
Air Force Materiel Command
United States Air Force

10. SPONSORING/MONITORING AGENCY ACRONYM(S)
AFRL/RZAS

11. SPONSORING/MONITORING AGENCY REPORT NUMBER(S)
AFRL-RZ-WP-TP-2008-2067

12. DISTRIBUTION/AVAILABILITY STATEMENT
Approved for public release; distribution unlimited.

13. SUPPLEMENTARY NOTES
PAO case number AFRL/WS07-1437, 18 June 2007. Presented at the 43rd AIAA/ASME/SAE/ASEE Joint Propulsion Conference and Exhibit, 8-12 July 2007, Cincinnati, OH. This is a work of the U.S. Government and is not subject to copyright protection in the United States. Document contains color.

14. ABSTRACT

Numerical studies were performed to examine different strut configurations to determine their mixing characteristics for possibly use with fuel-injector ports for round scram jet-combustor applications. Several strut configurations were tested to provide a better understanding of the flow physics, in terms of pressure, total pressure recovery, vorticity magnitude, streamlines, and velocity vectors. The conceptual strut designs were placed in a rectangular flow path, and the computations will be followed by an experimental program in the AFRL/RZA Research Cell 19 supersonic wind-tunnel facility, which has a rectangular cross-section area of 12.7 cm x 15.24 cm. The struts were sized, however, for eventual use in a 25.4 cm (10-inch) round combustor. The strut with a constant leading-edge angle and a moderately swept trailing edge seems to provide reasonably good mixing flow features without significantly compromising the total pressure recovery.

15. SUBJECT TERMS
Supersonic combustion, strut injection, flameholding.

16. SECURITY CLASSIFICATION OF:			17. LIMITATION OF ABSTRACT:	18. NUMBER OF PAGES	19a. NAME OF RESPONSIBLE PERSON (Monitor)
a. REPORT	b. ABSTRACT	c. THIS PAGE			Mark Gruber, Ph.D.
Unclassified	Unclassified	Unclassified	SAR	18	19b. TELEPHONE NUMBER *(Include Area Code)* (937) 255-7328

Standard Form 298 (Rev. 8-98)
Prescribed by ANSI Std. Z39-18

43rd AIAA/ASME/SAE/ASEE Joint Propulsion Conference & Exhibit
8 - 11 Jul 2007, Cincinnati, Ohio

AIAA-2007-5403

Aerodynamic Performance of an Injector Strut for a Round Scramjet Combustor

Chung-Jen Tam[¶]
Taitech, Inc., AFRL/PRAS, Wright-Patterson Air Force Base, OH 45433

Kuang-Yu Hsu[§]
ISSI, AFRL/PRAS, Wright-Patterson Air Force Base, OH 45433

Mark R. Gruber[†]
AFRL/PRAS, Wright-Patterson Air Force Base, OH 45433

and

Charbel N. Raffoul[‡]
AFRL/PRAT, Wright-Patterson Air Force Base, OH 45433

Numerical studies were performed to examine different strut configurations to determine their mixing characteristics for possibly use with fuel-injector ports for round scramjet-combustor applications. Several strut configurations were tested to provide a better understanding of the flow physics, in terms of pressure, total pressure recovery, vorticity magnitude, streamlines and velocity vectors. The conceptual strut designs were placed in a rectangular flow path, and the computations will be followed by an experimental program in the AFRL/PRA Research Cell 19 supersonic wind-tunnel facility, which has a rectangular cross-section area of 12.7 *cm* x 15.24 *cm*. The struts were sized, however, for eventual use in a 25.4 *cm* (10-inch) round combustor. The strut with a constant leading-edge angle and a moderately swept trailing edge seems to provide reasonably good mixing flow features without significantly compromising the total pressure recovery.

Nomenclature

H	=	strut height
L	=	strut length
M	=	Mach number
P_0	=	total pressure at the facility nozzle
RC	=	research cell
T_0	=	total temperature at the facility nozzle
W	=	strut width
x	=	streamwise direction
y^+	=	yv^*/v
z	=	normal direction to the bottom wall

I. Introduction

For large-scale scramjet-engine designs, one of the main challenges is the fuel-injection strategy, *i.e.*, the penetration and mixing characteristics of the fuel in the combustor. Injector designs must effectively enhance fuel penetration to produce rapid mixing and combustion of the fuel and air without excessive increase in jet-injection supply pressure, to achieve high fuel penetration into the core flow. In addition, injector designs and the flow disturbances produced by injection should provide a region for flame holding, and thus in a stable piloting source for

¶ Sr. Research Scientist, Taitech Inc., 1430 Oak Court, Suite 301, Beavercreek, OH 45430, Associate Fellow AIAA.
§ Sr. Research Scientist, ISSI., 2766 Indian Ripple Road, Beavercreek, OH 45430, Associate Fellow AIAA.
† Sr. Aerospace Engineer, AFRL/PRAS, WPAFB, OH 45433, Associate Fellow AIAA.
‡ Program Manager, AFRL/PRAT, WPAFB, OH 45433.

downstream ignition of the fuel. On the other hand, the fuel jets should not introduce additional total pressure losses. Thus, based on total pressure, jet-injection designs for scramjet-engine applications can be divided into two categories, *i.e*., non-intrusive and intrusive fuel jet-injection technologies. The non-intrusive designs mainly include flush-wall injectors to minimize the total pressure loss. These injectors can be classified by angle (normal, low-angled, and transverse),[1-4] shape (circular, elliptical, wedge, and diamond shaped),[5-8] and configuration (aeroramp, cascade, and swirl injectors).[9-16]

Intrusive concepts for fuel mixing enhancement include ramps, pylons, and struts.[17-21] These designs tend to create more aerodynamic disturbances than non-intrusive mechanisms, with an inevitable increase in total pressure losses and drag. Active cooling, with its associated complexities, is usually required for intrusive devices. Nevertheless, such designs do, in general, provide better fuel-air mixing in the scramjet combustor, and they could potentially enhance the combustion process, significantly reducing the required length of the scramjet engine. These benefits may well be great enough to outweigh the drawbacks.

This research focuses on the use of a strut-injection technique for a large-scale round scramjet combustor. Struts offer the possibility of injecting fuel directly into the core of a supersonic flow without using high pressure supply. On the other hand, since the strut is exposed to the main flow, the total pressure losses, heat flux and flow disturbance must be evaluated. Numerical studies were performed as a pre-test analysis to examine different strut configurations for better mixing flow features and optimize fueling schemes for round scramjet-combustor applications. Several leading-edge strut configurations were tested to provide a better understanding of the flow physics, in terms of pressure, total pressure recovery, vorticity magnitude, streamlines and velocity vectors. The conceptual single-strut designs were performed in a rectangular flow path, because the computations will be followed by an experimental program in the AFRL/PRA Research Cell 19 supersonic wind-tunnel facility at Wright-Patterson Air Force Base, OH, which has a rectangular cross-section area of 12.7 *cm* x 15.24 *cm*. The struts were sized for eventual use in a 25.4 *cm* (10-inch) round scramjet combustor.

II. Numerical Approach

All simulations were performed using the CFD^{++} code, a general-purpose CFD tool developed by Metacomp Technologies.[22] CFD^{++} uses a finite-volume numerical framework, with multi-dimensional TVD schemes and Riemann solvers for accurate representation of supersonic flows. Several types of Riemann solver are available; the HLLC Riemann solver with minmod flux limiting was used in the simulations described here. Multi-grid acceleration is available to provide a fast and accurate solution methodology for both steady and unsteady flows. A variety of one-, two-, and three-equation turbulence models are available for RANS calculations, along with large eddy simulation (LES) and hybrid RANS/LES options. Unless otherwise specified, turbulence was modeled using the two-equation cubic κ-ε model. This model has non-linear terms that account for normal-stress anisotropy, swirl and streamline curvature effects. At solid surfaces, an advanced two-layer wall function with equilibrium and non-equilibrium blending was employed to reduce grid requirements. Chemically reacting flows can be modeled with general finite-rate kinetics models. The code supports both structured (quadrilateral and hexahedral) and unstructured (triangle, prism, and tetrahedral) grids. An MPI is used to take advantage of modern parallel-processing computers. The numerical solutions were considered to be converged based on the residual history and the steadiness of the mass flow rate. The mass flow rate should not change, that is, it should be constant along the isolator.

Initial/Boundary Conditions and Grid

The conceptual strut configurations were simulated with inflow conditions of $M = 2$ with $T_0 = 294\ K$ and $P_0 = 344.7\ kPa$, corresponding to the test conditions available in the AFRL/PRA Research Cell 19 facility.[23] The supersonic wind tunnel is a direct-connect facility, that is, the test section is connected to the exit of the facility nozzle. The Research Cell 19 test section has a cross-section area of 12.7 *cm* x 15.24 *cm* (5″ x 6″) with a length of 63.5 *cm* (25″). The numerical simulations were extended from the facility nozzle plenum to the entrance of the test section to provide the inflow conditions for the test section, as illustrated in Figure 1. This practice obviates the use of ad-hoc profiles at the isolator entrance.

The experimental hardware available at the AFRL/PRA RC 19 wind-tunnel facility consists of a rectangular test section with a strut. Considering a 45° segment centered on the strut, this configuration will be used to represent one sector of an eight-strut configuration in a 25.4 *cm* (10″) round combustor, as shown in Figure 2. Due to the symmetry assumption at the centerline plane, only half of the strut configuration (and a 22.5° angle) was computed

in this study, as depicted in Figure 3. A no-slip, adiabatic boundary condition was imposed on the solid walls and the strut surfaces. A zero-gradient condition was applied at the isolator outflow plane.

The computational domains consisted of 2.6 million grid cells. The grid was clustered to all solid surfaces at a level appropriate for the use of wall functions ($y^+ \leq 70$). Although CFD^{++} allows unstructured grids, a structured-grid topology was used to provide better constant grid clusterings without significantly increasing the number of grid cells, particularly near the solid surfaces, as shown in Figure 4.

III. Results

Six different conceptual struts were tested numerically to determine their performance, in terms of total pressure recovery and mixing characteristics. Table 1 lists descriptions of the strut configurations. The tip of each strut is rectangular, triangular/rectangular or triangular, as shown in Figure 5. Each rectangular or triangular section is 1.27 *cm* (1/2″) in length, so that the total length for the triangular/rectangular tip is 2.54 *cm* (1″). Note that the total width of the strut designs is 0.9525 cm (3/8″), but due to the symmetry assumption only half of the strut width is simulated (Figure 5b). All of the struts were tested with a height of 2.54 *cm*; two were also tested with a height of 1.27 *cm*.

Figure 6 shows the pressure contours for the different strut configurations at the plane of symmetry, the bottom wall, and a cross-sectional plane at the trailing edge of the strut. The oblique-shock systems created by these strut designs are highly three-dimensional flow structures. A bow-shock-type system can be observed in the cross-sectional plane (Figure 6). Due to the intrusive nature of the current strut designs, the bow-shock structures in the vicinity of the trailing edge of the strut expand beyond the half-angle of the 45° constraint. In addition, the reflected shocks from the side and top walls of the rectangular flow path could compromise the flow physics downstream of the struts. The numerical results do, however, provide an understanding of the different flow phenomena in the immediate vicinity of the various conceptual strut configurations.

The flat surface of Strut A (Figure 5a) acts like a wedge, creating a strong oblique shock system at the leading edge. Thus, there is a sharp increase in pressure at the vicinity of the strut region, as shown in Figure 7. Consequently, the total pressure recovery is lower than that of the other strut configurations near the strut region. While it is relatively simple to manufacture, this strut design could experience high pressure and thermal stress at the leading edge, which could compromise, even fatally, the structural integrity of the strut. Strut configurations with different leading-edge angles were tested to reduce the strong oblique shock produced by Strut A. One group of designs has a variable leading-edge angle, and the other has a constant leading-edge angle, as depicted in Figure 4a and Figure 4b, respectively. One of the main benefits of the variable-angle leading-edge (Struts B and C) is that the angle is shallower than for the strut with constant angle. Hence the oblique shock induced from the leading edge is weaker and the total pressure recovery losses are lower. Both Struts B and C have the variable leading-edge angle design, but the sweep angle of Strut C is smaller than that of Strut B because Strut C has only a triangular tip section (all of the struts are 10.16 *cm* long). Therefore the oblique shock induced by the leading edge is weaker, and the total pressure recovery loss is lower for Strut C than for Strut B, as shown in Figure 7.

Numerical simulations were also performed using Struts B and C with a reduced height of 1.27 *cm*, to minimize the flow disturbance due to the oblique-shock system, and to decrease the area blockage of the strut. It was hoped that reducing the strut height would confine the flow structure induced by the strut to within a 45° angle, but it was found that the oblique-shock structures still expand beyond the constraint, as illustrated in Figure 8. Therefore no further effort was pursued to reduce the strut height. Any additional reduction in the height of the strut would make it too small to effectively provide fuel injection to the core flow.

The strut with a variable leading-edge angle might be expected to produce less flow disturbance, because of its smaller deflection angles from the base to the tip of the strut, as compared with the constant leading-edge angle design (Figure 4). This type of strut would, however, be challenging to design and fabricate. Since the leading-edge angle is not constant and is made of two non-congruent angles at different planes, the leading-edge surface of the strut is not a flat surface. Two designs with variable leading-edge angle were nevertheless considered (Figure 5b and c). The strut with a constant leading-edge angle (Figure 4b) has a sidewall consisting of two flat surfaces and would be relatively easy to fabricate and might be more cost-effective. Therefore several sizes of strut with a constant leading-edge angle were considered, as illustrated in Figure 5d-Figure 5f. The leading-edge portion of the struts is the same in these designs, although the strut bases have different lengths. Detailed descriptions of these struts are listed in Table 1.

The 3-D bow-shock structure is much stronger for Strut D, with the constant leading-edge angle, than for Strut B, as shown in Figure 6d and Figure 6b, respectively. This trend can be also observed from the separated-flow averaged pressure distributions along the strut region (Figure 7a), and thus in the total pressure recovery (Figure 7b). Another difference in flow features for these two designs is the pressure rise at the leading edge of the struts. For

Strut B, the pressure increases gradually from the base to the tip of the strut because of the increase in the deflection angle, as illustrated in Figure 6b and Figure 7a. On the other hand, for Strut D, since the leading-edge angle is constant and the deflection angle of the tip is the same as for Strut B, the pressure rise due to the oblique shock is quite strong and uniform (Figure 6d and Figure 7a). The flow then expands rapidly at the strut sidewall, particularly at the upper portion, as shown in Figure 6d. This is primarily due to the sweep angle, which causes the flow to expand away from the corner junctions between the sidewall of the strut and bottom wall. In addition, the flow is expanded not only at the side of the strut, but also at the tip and the trailing edge of the strut. These flow-expansion phenomena combine to create very complex flow features downstream of the strut. The flow physics of this strut will be discussed with reference to the two other similar strut designs in the following section.

The length of the strut base was shortened to improve the performance of the Strut D design, as depicted in Figure 5e and Figure 5f. Decreasing the strut length at the base also reduces the surface area at the side of the strut, which allows the flow to expand earlier along the trailing edge of the strut, particularly from the strut base (Figure 7a). In addition, this flow characteristic reduces the total pressure loss (Figure 7b), as in the cases of Struts E and F. With the smallest surface area (Strut F), the pressure rise and total pressure loss are obviously smaller than those of the other two designs. Among the three struts with constant leading-edge angle, Strut E seems to provide better mixing flow features, as evidenced by the stronger vorticity magnitude contours, as illustrated in Figure 9. The vorticity contours are shown in four different planes; symmetry, x = 1.0036 *m* (2.54 *cm* downstream of the trailing edge of the strut tip), and z = 1.27 and 2.54 *cm* away from the bottom wall. There is a distinct strong upward vorticity or shear flow at the plane of symmetry for Struts E and F. This feature can be clearly seen in the 3-D view of the streamlines (Figure 9b and Figure 9c). The streamlines show a strong upward vortical motion toward the tip of the strut trailing edge, which causes the flow at the tip of the strut trailing edge to deflect upward. In contrast, a downward motion due to strong expansion in the region is seen with Strut D (Figure 9a). In the case of Strut D, the vorticity is confined within the tip of the strut, and its downstream intensity at x = 1.0036 *m* is much weaker than that of the other two designs. In all three cases, the flow is turned upward after the leading edge due to the sweep angle. This feature is most apparent from the first streamline away from the bottom wall, as shown in Figure 9. This streamline tends to follow the low pressure region along the sidewall of the strut in the vertical direction (Figure 6d-Figure 6f). Note that two sets of streamlines were emitted upstream of the strut. One set was located at the symmetry plane and the other set of streamlines was drawn from 0.7 *mm* away. The color of the streamlines is associated with the local Mach number. Since the trailing edge of Strut D is not swept, as in Struts E and F, the flow does not have a strong upward component in the wake region. In addition, due to the strong expansion at the tip of the trailing edge (Figure 10a), the flow behind the strut becomes a large wake region, which can be observed from the vorticity contours in the z-direction cross-sectional planes (z = 1.27 and 2.54 *cm*) and the velocity vectors, as shown in Figure 9a and Figure 10a, respectively. On the other hand, with the trailing swept edge, as in Struts E and F, the flow turns upward at the trailing edges, and creates a strong upward vortex structure (Figure 9b and Figure 9c). The upward motion of the flow can be seen from the velocity vectors behind the struts, as depicted in Figure 10b and Figure 10c. Unlike Strut D, the flow in the upward direction behind the strut is stronger than the incoming flow from the tip, which creates an oblique shock instead of an expansion wave (Figure 10b and Figure 10c). These flow phenomena could explain the strong upward vorticity or shear layer in that region, as observed in Figure 9b and Figure 9c.

An important difference in the flow features for Struts E and F is the vortical structure. The vorticity is stronger for Strut E than for Strut F, particularly downstream of the strut region at x = 1.0036 *m* (Figure 9b and Figure 9c). This could be caused by the thicker boundary layer formed on the larger sidewall surface area in Strut E. As the flow expands at the trailing edge of the strut, the velocity gradient at the shear layer becomes larger and consequently the magnitude of the vorticity also increases. This can be observed at z = 2.54 *cm* shown in Figure 9b. This indicates that Strut E has a larger wake region behind the trailing edge than does Strut F, as shown in Figure 10b and Figure 10c, respectively. A similar observation can be seen from the pressure contours in Figure 6e and Figure 6f. The results indicate that to enhance the mixing characteristic of a strut, the trailing-edge of the strut needs to be swept to create an upward motion. At the same time, the sweep angle can be too small, as in Strut F, which could potentially reduce the wake region behind the strut and diminish its mixing capability. Overall, Strut E seems to provide better mixing characteristics. Recent experimental work[20] also indicates that struts with a swept trailing edge provide better mixing than do struts with normal trailing edges, like Strut D.

IV. Conclusions

Three different leading-edge strut configurations were tested numerically to determine their performance, in terms of total pressure recovery and mixing characteristics. The designs include a flat surface, and variable and constant leading-edge angles. Although the struts with variable leading-edge angles provide lower total pressure

loss, they could be hard to fabricate because the leading-edge surface is not a flat surface. Struts with a constant leading-edge angle and different sweep angles at the trailing edge were simulated to understand their mixing characteristics. Strut E was found to potentially offer relatively good mixing capability without a significant penalty in total pressure recovery. In addition, this strut could be relatively easy to fabricate.

V. Future Work

The experimental program to validate the computations will be performed in the AFRL/PRA Research Cell 19 supersonic wind tunnel at Wright-Patterson Air Force Base, OH. In the future, however, struts like these might be used as part of an eight-strut fuel-injector configuration in round combustors. The struts were therefore scaled so that they might be used in a future 10-inch round combustor, and the behavior of the flow within a 45° section was especially considered. Obviously, a conclusion drawn about flow structures around a strut in a rectangular wind tunnel will be only marginally applicable to round tunnels. Since round combustors are currently of considerable interest, however, and rectangular wind tunnels are most widely available for testing, it is a matter of some urgency to explore comparisons between the two. In addition, rectangular flow path provides easy optical access for any flow diagnostics.

Based on the numerical simulations, recommendations will be made to determine possible locations on the strut for fuel-injector ports.

VI. Acknowledgments

This study was supported by and performed at Wright-Patterson Air Force Base, under Contract F33615-03-D-2419 TO 002. The support for this project is sincerely appreciated. Additional support took the form of a grant of computer resources from the ASC and ERDC Department of Defense High Performance Computing Center. The authors would also like to thank Dr. Daniel Risha of AFRL/PRAT for his invaluable technical discussion, and Anna Creese of Taitech for her editorial consultation.

VII. References

1. Fuller, R.P., Wu, P.-K., Kirkendall, K.A., and Nejad, A.S., "Effects of Injection Angle on Atomization of Liquid Jets in Transverse Airflow," *AIAA Journal*, Vol. 38, No. 1, 2000, pp. 64-72.
2. Ali, M. and Sadrul Islam, A.K.M., "Study on Main Flow and Fuel Injector Configurations for Scramjet Applications," *International Journal of Heat and Mass Transfer*, Vol. 49, 2006, pp. 3634–3644.
3. Lewis, D.P. and Schetz, J.A., "Tangential Injection from Overlaid Slots into a Supersonic Stream," *Journal of Propulsion and Power*, Vol. 13, No. 1, 1997, pp. 59-63.
4. Rowan, S.A. and Paull, A., "Performance of a Scramjet Combustor with Combined Normal and Tangential Fuel Injection," AIAA Paper 2005-0615, 2005.
5. Gruber, M.R., Nejad, A.S., Chen, T.H., and Dutton, J.C., "Transverse Injection from Circular and Elliptical Nozzles into a Supersonic Crossflow," *Journal of Propulsion and Power*, Vol. 16, No. 3, 2000, pp. 449-457.
6. Barber, M.J., Schetz, J.A., and Roe, L.A., "Normal, Sonic Helium Injection Through a Wedge-Shaped Orifice into Supersonic Flow," *Journal of Propulsion and Power*, Vol. 13, No. 2, 1997, pp. 257-263.
7. Tomioka, S., Jacobsen, L.S., and Schetz, J.A., "Sonic Injection from Diamond-Shaped Orifices into a Supersonic Crossflow," *Journal of Propulsion and Power*, Vol. 19, No. 1, 2003, pp. 104-114.
8. Grossman, P., Maddalena, L., and. Schetz, J.A., "Wall Injectors for High Mach Number Scramjets," AIAA Paper 2006-4682. 2006.
9. Jacobsen, L.S., Gallimore, S., Schetz, J.A., O'Brien, W., and Goss, L., "Improved Aerodynamic-Ramp Injector in Supersonic Flow," *Journal of Propulsion and Power*, Vol. 19, No. 4, July-August 2003.
10. Lee, S.-H., "Characteristics of Dual Transverse Injection in Scramjet Combustor, Part 2: Combustion," *Journal of Propulsion and Power*, Vol. 22, No. 5, 2006, pp. 1020-1026.
11. Price, B.B., Elliot, G.S., and Ogot, M., "Experimental Optimization of Transverse Jet Injector Geometries for Mixing into a Supersonic Flow," AIAA Paper 1998-3019, 1998.
12. Mathur, T., Cox-Stouffer, S.K., Hsu. K.-Y., Crafton, J., Donbar, J.M., and Gruber, M.R., "Experimental Assessment of a Fuel Injector for Scramjet Applications," AIAA Paper 2000-3703, 2000.
13. Cox-Stouffer, S.K., Gruber, M.R., and Bulman, M.J., "A Streamlined, Pressure-Matched Fuel Injector for Scramjet Applications," AIAA Paper 2000-3707, 2000.

14. Kobayashi, K., Tomioka, S., Kato, K., Murakami, A., and Kudo, K., "Performance of a Dual-Mode Combustor with Multistaged Fuel Injection," *Journal of Propulsion and Power*, Vol. 22, No. 3, 2006, pp. 518-526.
15. Takahashi, S., Sato, N., Tsue, M., Kono, M., Nakamura, M., Kondo, H., and Ujiie, Y., "Control of Flame-Holding in Supersonic Airflow by Secondary Air Injection," *Journal of Propulsion and Power*, Vol. 14, No. 1, 1998, pp. 18-23.
16. Cutler, A.D. and Doerner, S.E., "Effects of Swirl and Skew Upon Supersonic Wall Jet in Crossflow," *Journal of Propulsion and Power*, Vol. 17, No. 6, 2001, pp. 1327-1332.
17. Kawano, S., Aso, S., and Orino, M., "A Study of a New Injector for Improvement of Supersonic Mixing," AIAA Paper 2000-0089, Jan. 2000.
18. Shreenivasan, O., Kumar, R., Kumar, T., Sujith, R., and Chakravarthy, S., "Mixing in Confined Supersonic Flow Past Strut Based Cavity and Ramps," AIAA Paper 2004-4194, 2004.
19. Manoharan, S., Chandra, B., Chakravarthy, S., Ramakrishnan, S., and Subramanyam, J., "Experimental Studies of Supersonic Cold Flow Mixing with Ramp Mixers," *Journal of Aerospace Engineering*, Vol. 18, No. 4, Oct. 2005, pp. 197-205.
20. Hsu, K.-Y., Carter, C., Gruber, M., and Barhorst, T., "Experimental Study of Cavity-Strut Combustion in Supersonic Flow," AIAA Paper 2007-5394, 2007.
21. Doster, J., King, P., Gruber, M., Maple, R., "Pylon Fuel Injector Design for a Scramjet Combustor," AIAA Paper 2007-5404, 2007.
22. Metacomp, http://www.metacomptech.com/index.html, 2006.
23. Gruber, M.R. and Nejad, A.S., "New Supersonic Combustion Research Facility," *Journal of Propulsion and Power*, Vol.11, No.5, 1995, pp.1080-1083.

Strut	Descriptions of the strut	Length *cm*	Height *cm*	Width *cm*
A	Flat leading edge with a rectangular tip	10.16	2.54	0.4763
B	Variable leading-edge angle with a triangular/rectangular tip	10.16	1.27, 2.54	0.4763
C	Variable leading-edge angle with a triangular tip	10.16	1.27, 2.54	0.4763
D	Constant leading-edge angle with a triangular/rectangular tip	10.16	2.54	0.4763
E	Constant leading-edge angle with a triangular/rectangular tip	5.08	2.54	0.4763
F	Constant leading-edge angle with a triangular/rectangular tip	2.54	2.54	0.4763

Table 1 Descriptions of the conceptual strut designs.

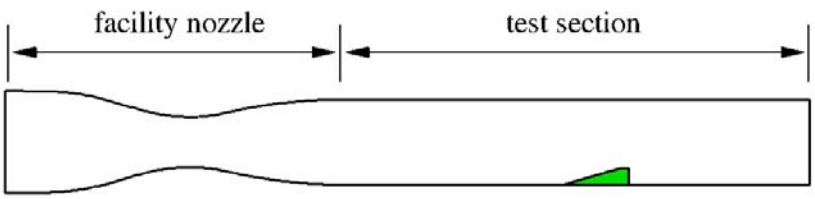

Figure 1 Schematic of AFRL/PRA RC 19 supersonic wind-tunnel facility and strut location.

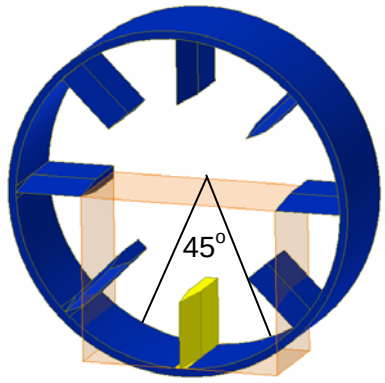

Figure 2 A single strut in a 12.7 *cm* x 15.24 *cm* (5" x 6") rectangular flow path with a 25.4 *cm* (10") round combustor with eight-strut injection overly.

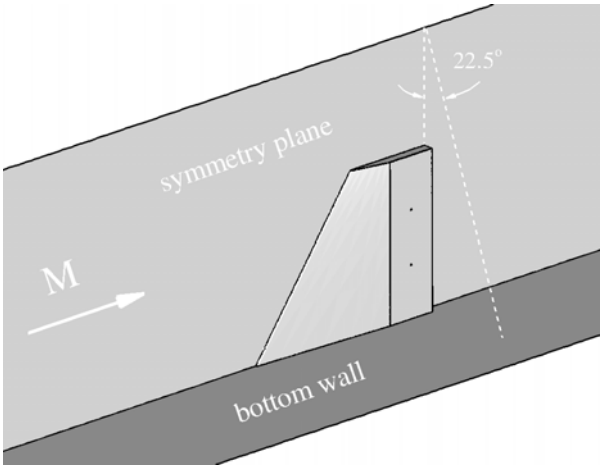

Figure 3 Computational domain of a single strut in a rectangular combustor flow path.

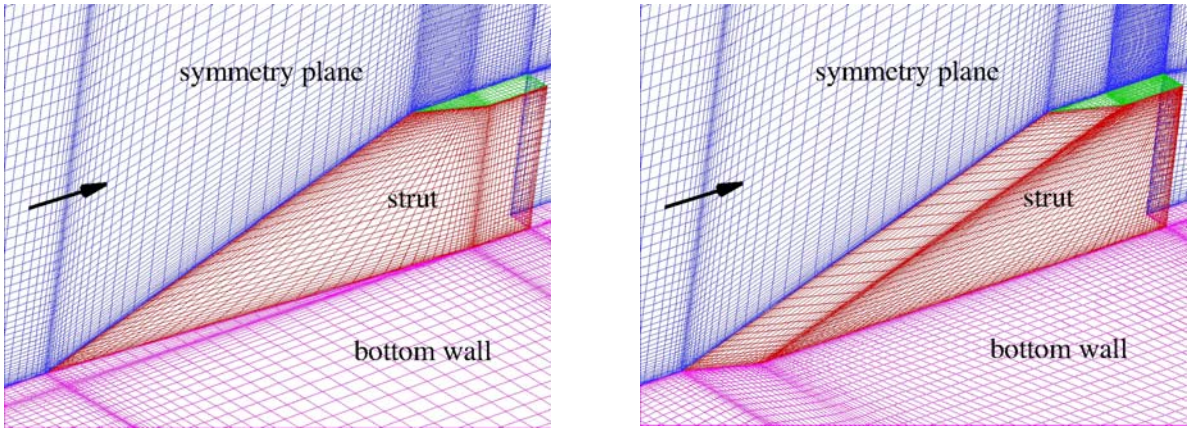

(a) Strut with variable leading-edge angle (b) Strut with constant leading-edge angle

Figure 4 Computational topologies near the vicinity of the strut.

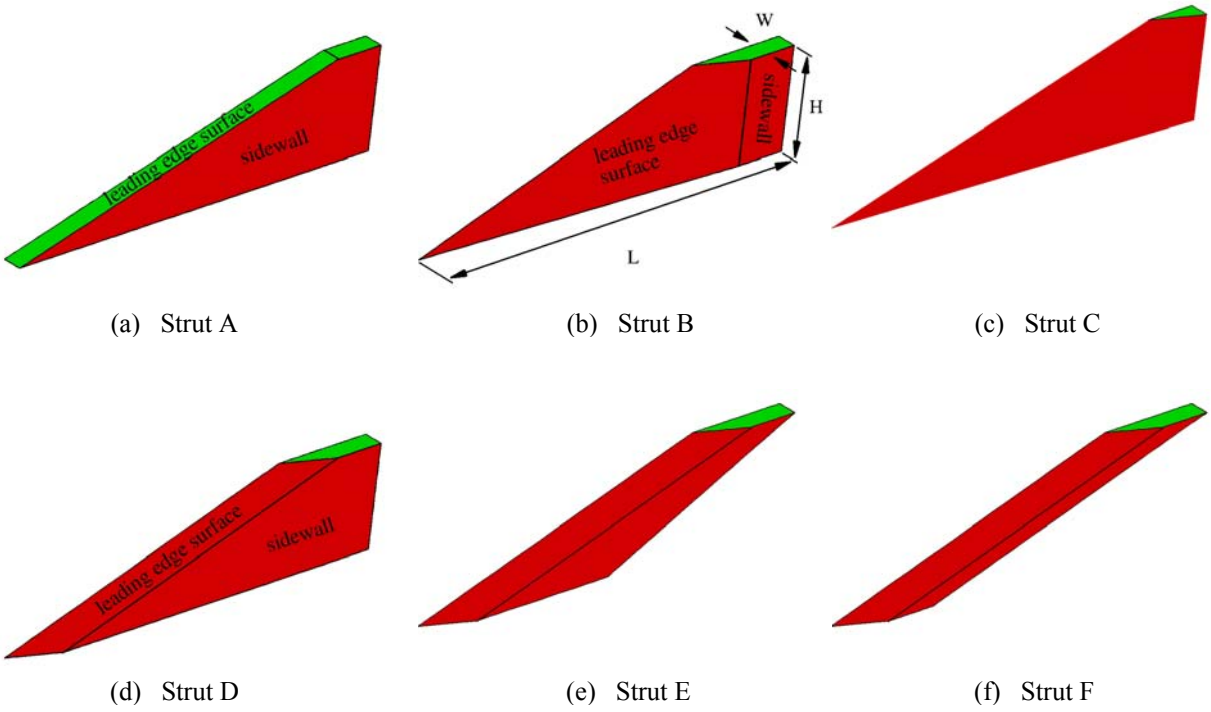

(a) Strut A (b) Strut B (c) Strut C

(d) Strut D (e) Strut E (f) Strut F

Figure 5 Conceptual strut configurations.

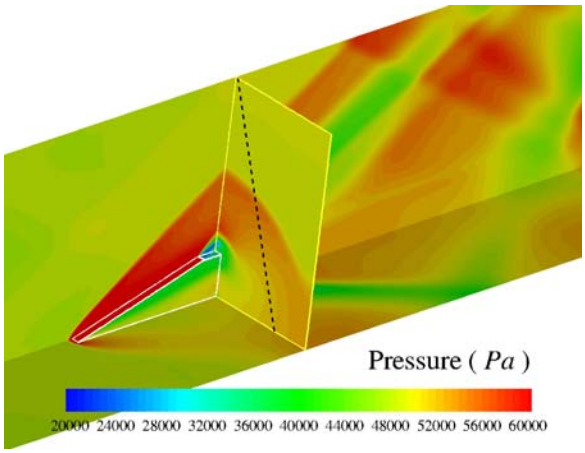

(a) Strut A

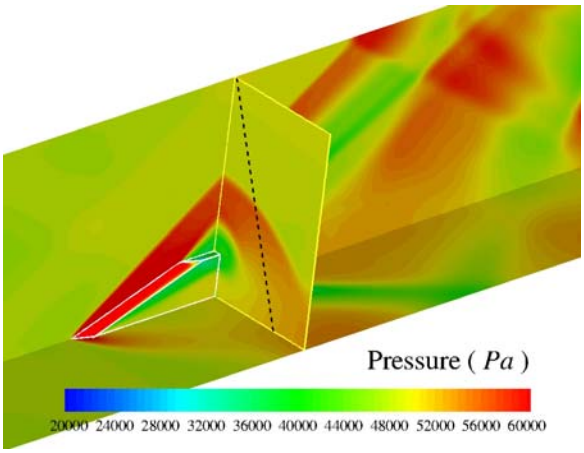

(d) Strut D

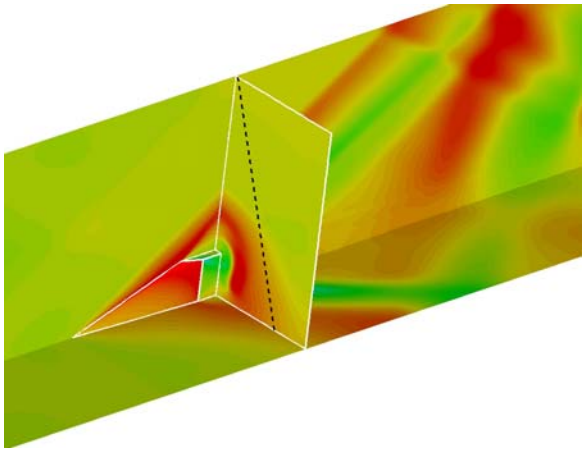

(b) Strut B

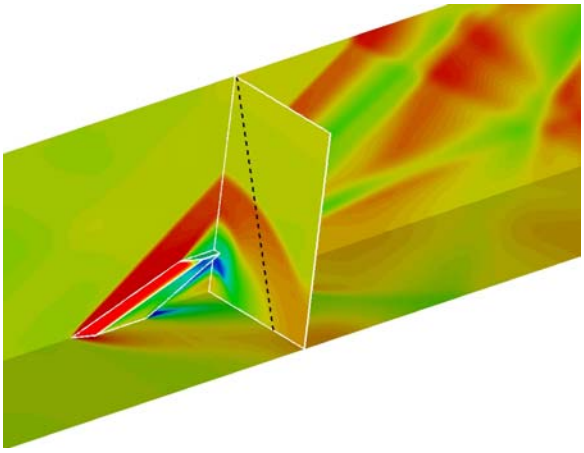

(e) Strut E

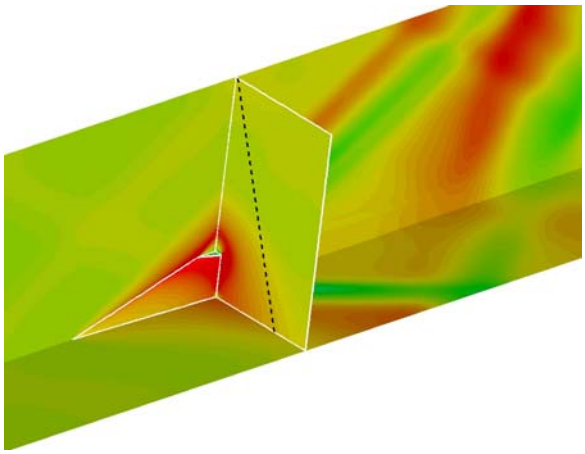

(c) Strut C

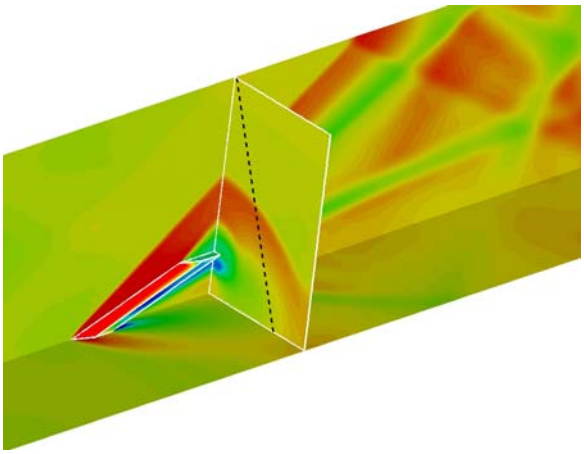

(f) Strut F

Figure 6 Static pressure contours for various strut configurations (dashed line represents 22.5° constraint).

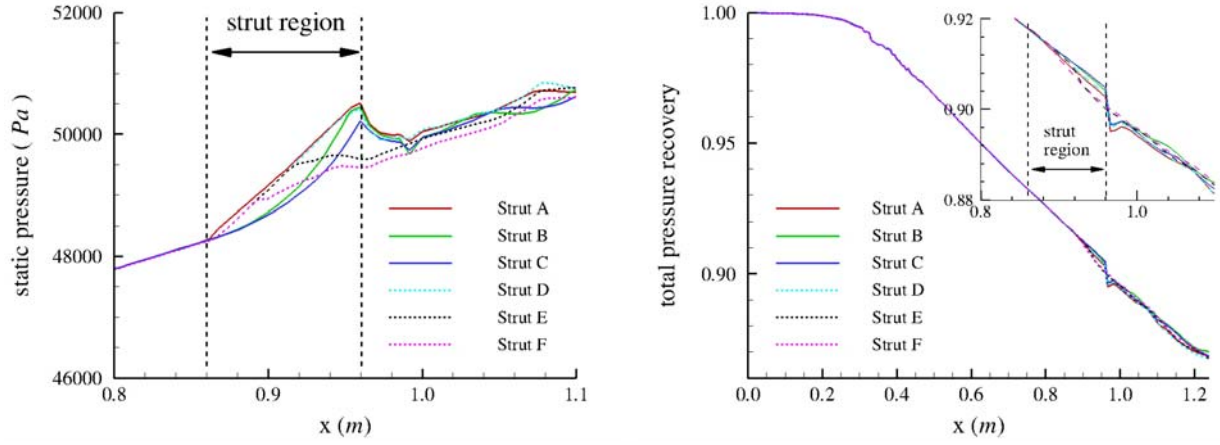

(a) Static pressure distribution (b) Total pressure recovery distribution

Figure 7 Separated-flow averaged quantities for various strut configurations.

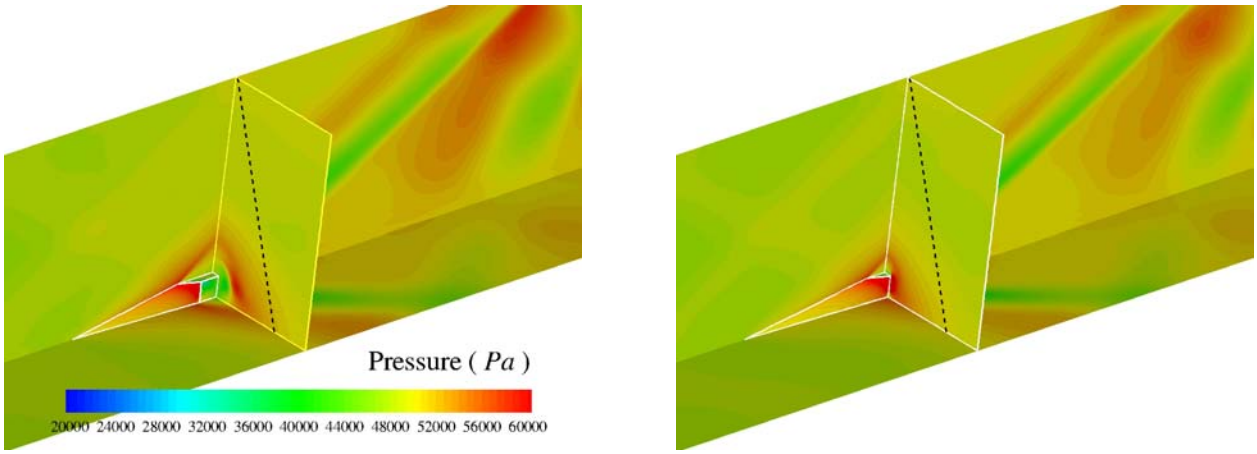

(a) Strut B (b) Strut C

Figure 8 Static pressure contours for Struts B and C with 1.27 *cm* (1/2″) height.

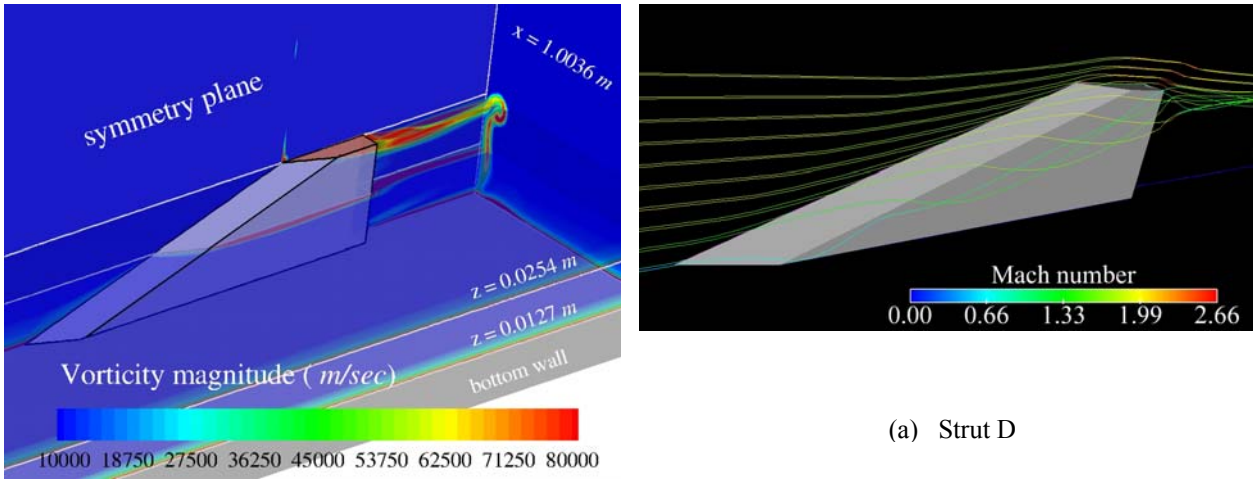

(a) Strut D

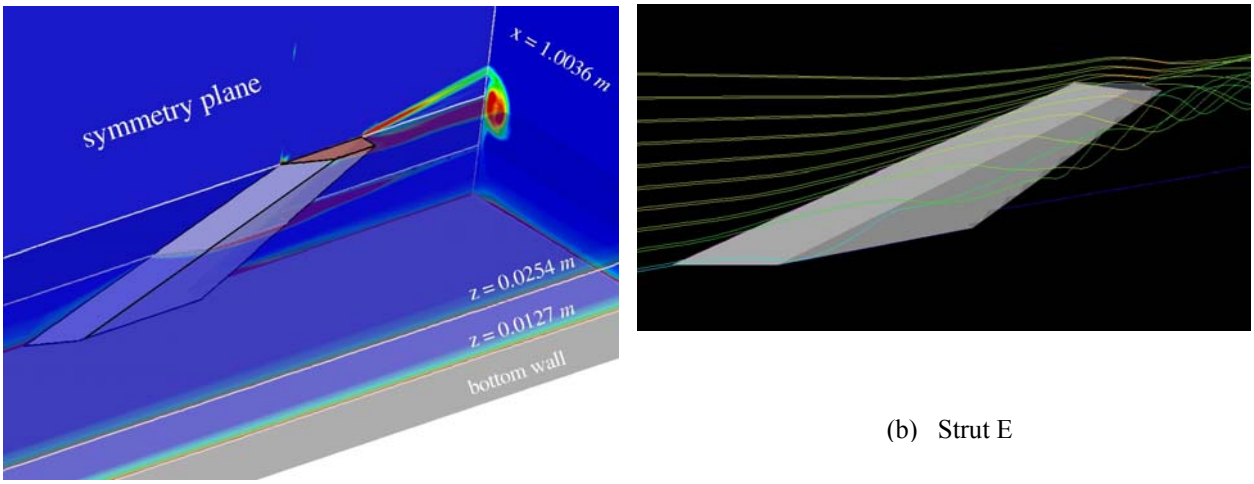

(b) Strut E

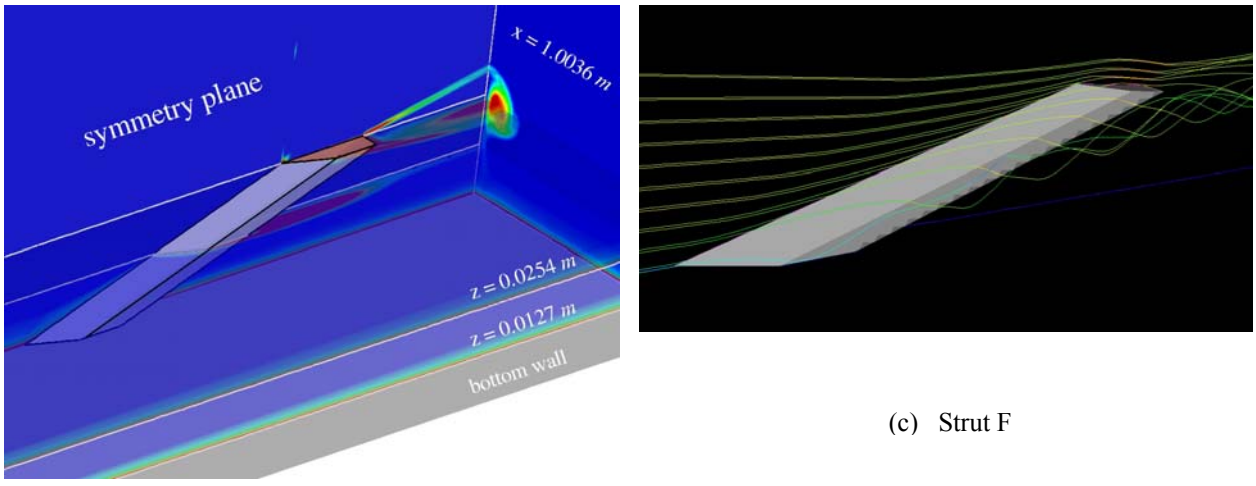

(c) Strut F

Figure 9 Vorticity magnitude contours and streamlines with Mach number for struts with constant leading-edge angle.

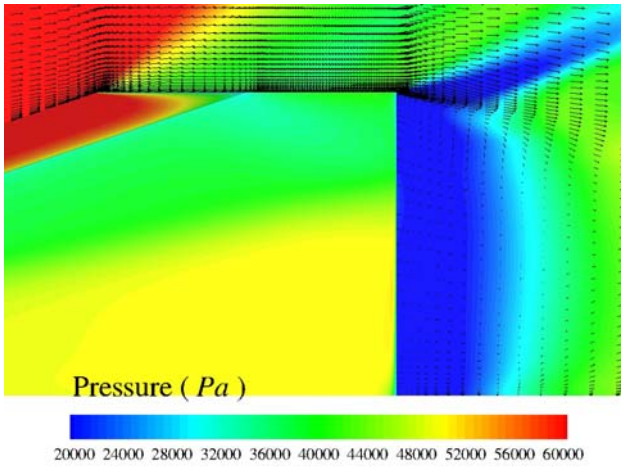

(a) Strut D

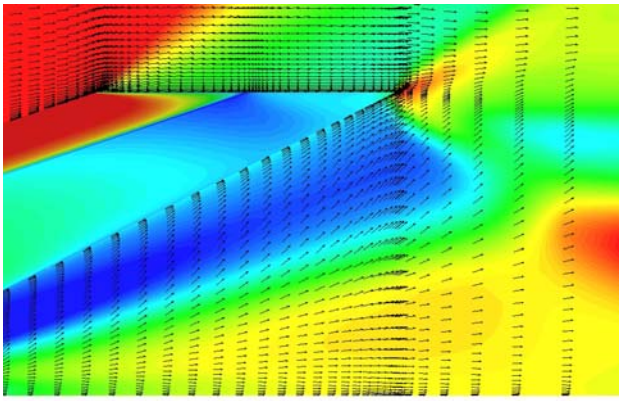

(b) Strut E

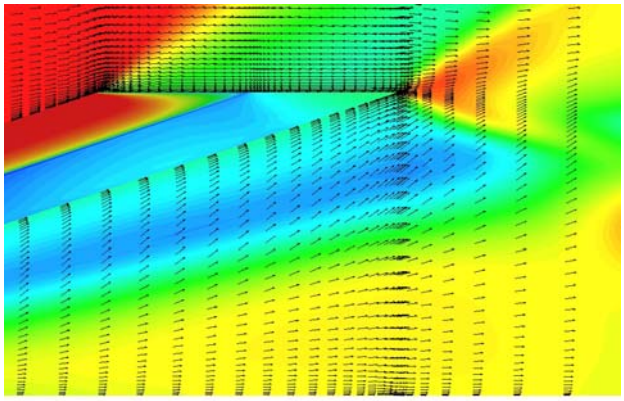

(c) Strut F

Figure 10 Velocity vectors and static pressure contours near the tips of the struts at the symmetry plane.